Hindawi
Advances in Civil Engineering
Volume 2023, Article ID 8262901, 18 pages
https://doi.org/10.1155/2023/8262901

Research Article

Simplified Calculation Method for the Natural Frequencies of the Offshore Wind Turbine Structures with Monopile Foundations Based on Euler–Bernoulli Beam Theory

Yanpei Jiang, Xiaomin Zhou, and Yong Liu

School of Civil and Resource Engineering, University of Science and Technology Beijing, Beijing 100083, China

Correspondence should be addressed to Xiaomin Zhou; groupzhou@163.com

Received 14 February 2023; Revised 3 June 2023; Accepted 6 June 2023; Published 28 July 2023

Academic Editor: Agathoklis Giaralis

The wind and wave loads on the offshore wind-turbine (OWT) structures with monopile foundations occur at specific frequencies. When these excitation frequencies are close to the natural frequencies of OWT structures, resonance can disturb the proper operation of the power-generation equipment and shorten the service life of the structural system. Therefore, to ensure safe and efficient operation, the natural frequencies of the OWT structures with monopile foundations must be determined. To this end, a calculation method for the natural frequencies of the OWT structures with monopile foundations is proposed. This method, which considers the mass ratio (the ratio of the lumped mass on the top of the tower to the total mass of the tower, the transition piece, and the monopile above the mudline) as well as the nonuniform moment of inertia of the structures above the mudline and the soil–structure interaction (SSI), is derived using the Euler–Bernoulli beam differential equation and slope-displacement equation of a monopile according to the flexibility matrix, stiffness equivalent principle, and virtual work principle. Finally, the natural frequency calculation method is compared with finite element simulation and other calculation methods.

1. Introduction

At the Paris Climate Conference in 2015, more than 190 countries negotiated an agreement to curtail climate change, hoping to replace fossil fuels with green energy worldwide [1]. Moreover, sustainable development policies promote the transition from traditional energy to new energy [2]. In addition, the gradual depletion of hydrocarbon reserves is pushing the energy market toward a clean and sustainable path [3]. As a potential clean energy alternative, wind-energy technology is gradually shifting from onshore to offshore. Compared with similar onshore technologies, offshore wind energy technology has certain advantages [4], including higher wind velocity, larger wind turbines, and broader installation areas. In recent years, as the costs have decreased and generator dimensions and power have increased, offshore wind power consumption has increased significantly [5]. Based on the price in 2017, the cost per MW-hour of offshore wind farms is lower than that of nuclear power plants, and it can become competitive to natural gas and other energy sources in the near future [6].

Among offshore wind power support structures, the monopile option is the most prevalent, accounting for approximately 80% of the installed support structures [7]. The monopile foundation is an economical option for offshore wind power [8]. A monopile is a simple pipe segment driven into the seabed, and its advantages include easy production and installation as well as low-construction cost and risk [9]. The main loads on offshore wind turbines (OWTs) are of dynamic or cyclic nature, which makes the support structure highly sensitive to dynamic loads [10]. Therefore, it is important to fully understand the structural frequency and adjust the natural frequency of the structure and its components during the design stage [11]. By adjusting the natural frequency, the resonance caused by the wind, waves, and wind turbine operation can be avoided, and the service life of the structure can be prolonged. The wind, wave, and operating frequencies of the wind turbines are shown in Figure 1.

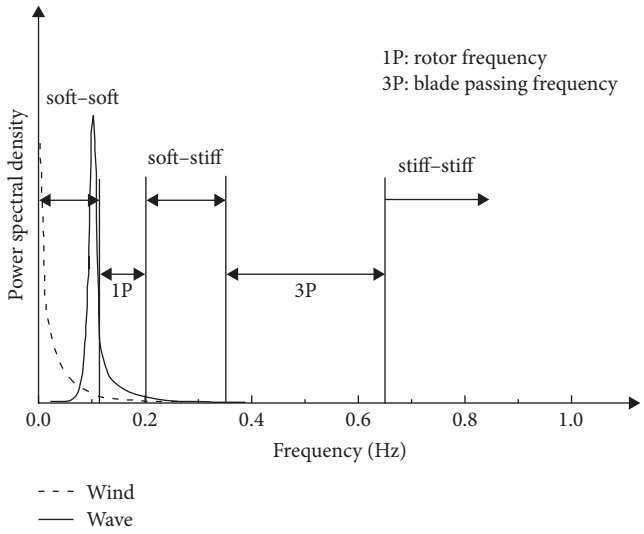

FIGURE 1: Wind, wave, and operation frequencies of an OWT.

Currently, the structural designs are either soft–soft, soft–stiff, or stiff–stiff. The soft–soft design is used for frequencies below 1P, the soft–stiff design is used for frequencies between 1 and 3P, and the stiff–stiff design is used for frequencies above 3P [11]. With the soft–soft design, the structure tends to be excessively deformed, which can affect the operation of the OWT, and the natural frequency of the structure can become close to the frequency of the external wind and wave loads, resulting in resonance. With the stiff–stiff design, more structural steel is used, which increases the costs. Most of monopile OWTs adopt soft–stiff design to reduce the construction costs [12]. When monopiles are used for large-size turbines, it is difficult for the designer to avoid the soft–soft design [13]. Another design strategy for OWTs, which are becoming increasingly larger in size (with a consequent shift of the natural frequency toward the resonance range), is the implementation of vibration control devices [14–35].

The frequency corresponding to the first-order bending vibration type is closer to the 1P frequency than to the 3P frequency. Moreover, under the action of wind, wave, and tide loads, offshore wind turbine structures swing back and forth and sideways, exhibiting a swinging pattern similar to that of the first-order bending vibration type. That is, the wind, wave, and tide loads stimulate the first-order bending vibration of offshore wind turbine structures. Therefore, in this study, the frequency corresponding to the first-order bending vibration of the structure was considered.

Natural frequency calculation methods include numerical and simplified calculation methods. Owing to their overall complexity, numerical calculations require computer programming. However, in terms of a simplified calculation method for the natural frequency, a calculator or spreadsheet program can be used.

Using an elastically supported Euler–Bernoulli beam, Adhikari et al. [36] derived the characteristic equation that controls the natural frequency of the structure and proposed a simplified calculation method for the frequency of OWTs considering the monopile. Arany et al. [37] studied the frequency of the OWTs with monopile foundations using mechanical and mathematical models and provided an approximation calculation formula for the natural frequency. Similarly, Arany et al. [10] proposed a simple calculation method for the natural frequency of the OWTs with monopile foundations based on the dimensions of the tower and monopile as well as the soil properties. Darvishi-Alamouti et al. [1] established a mathematical model for the soil–pile interaction based on Winkler's method and the concept of elastic foundation beams derived a simplified calculation method for the natural frequency of the OWTs with monopile foundations using the Rayleigh method of total energy conservation of the system. Ko [38] derived a closed-form solution for the natural frequency of the wind turbine structures with tapered towers based on Rayleigh's method.

There are also deficiencies in the methodologies reported in the literature [1, 10, 36–38]. Many researchers have used a simplified treatment of the upper tower [10, 36, 37], together with a large number of parameters and a narrow application scope. Darvishi-Alamouti et al.'s methodology [1] is applicable to cohesionless soils. However, Ko's methodology [38] is only applicable to tapered towers. To avoid such oversights, in this study, a natural frequency calculation method is established that reasonably considers the variation of upper tower diameter and wall thickness, has a wide application range and clearer dynamic principles, and is applicable to different soils.

2. Calculation Method for the Natural Frequency of the OWT Structures with Monopile Foundations

2.1. Natural Frequency for a Structure with a Fixed Support. First, a natural-frequency calculation method that does not consider monopiles and soil below the mudline is proposed. The ideal dynamic model of OWTs with monopile foundations is shown in Figure 2.

The undamped free vibration equation for the motion of Euler beams [39] is as follows:

$$\overline{m}\frac{\partial^2 v(z,t)}{\partial t^2} + E_t I_t \frac{\partial^4 v(z,t)}{\partial z^4} = 0, \tag{1}$$

where $\overline{m}$ is the mass per unit length, E_t is the elastic modulus of the structure, I_t is the moment of inertia, t is time, and z is the space coordinate.

Suppose that the solution of the above equation has the following form:

$$v(z,t) = X(z)Y(t). \tag{2}$$

Substituting Equation (2) into Equation (1) gives

$$\frac{\overline{m}}{E_t I_t} X(z)Y''(t) + X^{(4)}(z)Y(t) = 0. \tag{3}$$

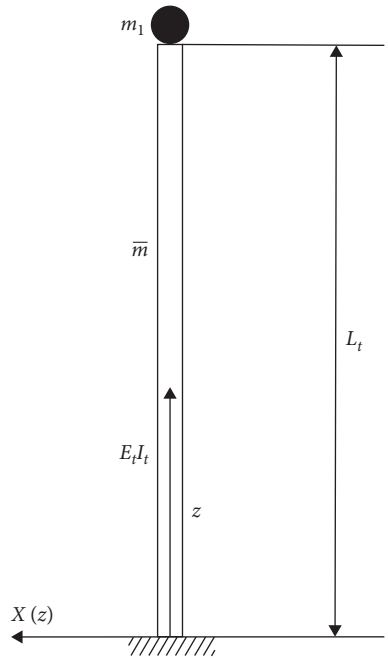

FIGURE 2: Dynamic model of an OWT.

Separating the variables in the above equation yields

$$\frac{\overline{m}}{E_tI_t}\frac{Y''(t)}{Y(t)} + \frac{X^{(4)}(z)}{X(z)} = 0. \tag{4}$$

To make the above equation valid, the following equation must be satisfied as follows:

$$\frac{X^{(4)}(z)}{X(z)} = -\frac{\overline{m}}{E_tI_t}\frac{Y''(t)}{Y(t)} = a^4. \tag{5}$$

Using the above equation, two ordinary differential equations and circular frequency expressions are obtained as follows:

$$Y''(t) + \omega^2 Y(t) = 0, \tag{6}$$

$$X^{(4)}(z) - a^4 X(z) = 0, \tag{7}$$

$$\omega^2 = \frac{a^4 E_tI_t}{\overline{m}}. \tag{8}$$

To determine the circular frequency from Equation (8), the differential Equation (7) must be solved, and the solution can be expressed as follows:

$$X(z) = A_1 \cos az + A_2 \sin az + A_3 \cosh az + A_4 \sinh az. \tag{9}$$

According to the boundary conditions of the displacement, shear force, bending moment, and slope in Figure 2, the following transcendental equation can be derived as follows:

$$\begin{aligned}&\cos^2(aL_t) + \cosh^2(aL_t) + \sin^2(aL_t) - \sinh^2(aL_t)\\ &+ 2\cos(aL_t)\cosh(aL_t)\\ &+ 2a\frac{m_1}{\overline{m}}\cos(aL_t)\sinh(aL_t)\\ &- 2a\frac{m_1}{\overline{m}}\cosh(aL_t)\sin(aL_t) = 0.\end{aligned} \tag{10}$$

By substituting $m_1/\overline{m} = \mu L_t$ and $aL_t = J$ into Equation (10), the following simplified equation is derived as follows:

$$\begin{aligned}&\cos^2(J) + \cosh^2(J) + \sin^2(J) - \sinh^2(J) + 2\cos(J)\cosh(J)\\ &+ 2J\mu\cos(J)\sinh(J) - 2J\mu\cosh(J)\sin(J) = 0,\end{aligned} \tag{11}$$

where $\mu = m_1/\overline{m}L_t$; μ is the ratio of the lumped mass on the top of the tower (total mass of the nacelle, hub, and blade) to the total mass of the tower, transition piece, and monopile above the mudline. Substituting the $aL_t = J$ into Equation (8) yields

$$\omega = J^2\sqrt{\frac{E_tI_t}{\overline{m}L_t^4}}. \tag{12}$$

The natural frequency of OWT structures with monopile foundations can be expressed as follows:

$$f = \frac{\omega}{2\pi} = \frac{J^2}{2\pi}\sqrt{\frac{E_tI_t}{\overline{m}L_t^4}}. \tag{13}$$

Here, the J value can be solved with the coefficient μ corresponding to different OWT structures using Equation (11). To obtain the natural frequency, the J value must be the first solution to the transcendental Equation (11). By substituting the J value into Equation (13), the structural natural frequency without considering the soil–structure interaction (SSI) can be derived. The J values corresponding to μ are shown in Figure 3.

A monopile-supported OWT structure usually has a nonuniform moment of inertia due to variations in tower diameter and tower wall thickness, the presence of the transition piece, and the monopile wall being thicker than the tower wall. As Equation (13) is applicable only for a uniform moment of inertia, it must be corrected.

(1) Moment of inertia

The structure shown in Figure 4 is clearly divided into three segments: $0\sim l_1$, $l_1\sim l_2$, and $l_2\sim l_3$. There is unnoticeable change in the diameter and wall thickness of segment $l_1\sim l_2$, whereas there is a noticeable change in the diameter and wall thickness of segment $l_2\sim l_3$. Therefore, it is necessary to consider the changes in the diameter and wall thickness of the tower based on the two sections when calculating the moment of inertia of the tower.

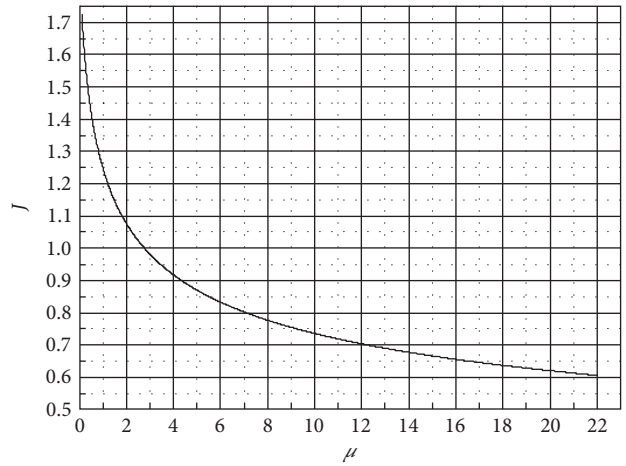

FIGURE 3: J value corresponding to μ.

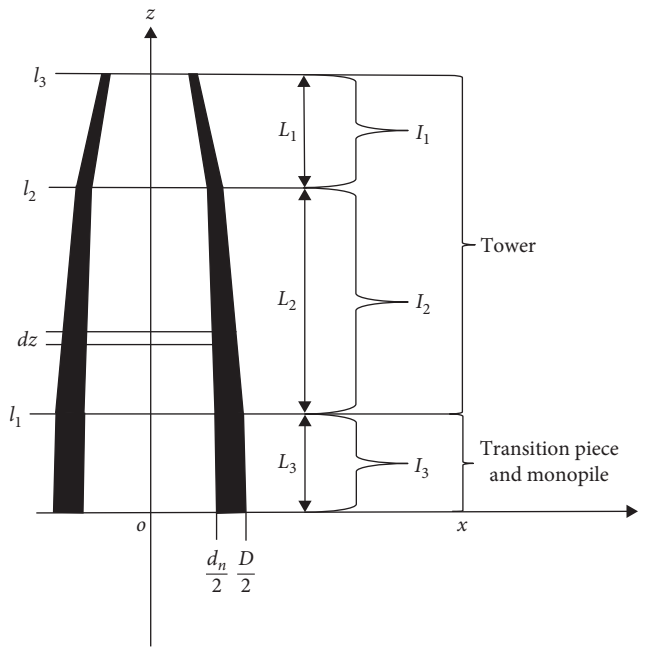

FIGURE 4: Structural profile.

From Figure 4, the outer diameter function can be expressed as follows:

$$D = F_1(z), \tag{14}$$

and the inner diameter function can be expressed as

$$d_n = F_2(z). \tag{15}$$

D and d_n are functions of z; therefore, the moment of inertia I_t can be expressed as a function of z:

$$I_t = f(z). \tag{16}$$

The weight number of the microelements in segment $l_1 \sim l_2$ in Figure 4 is given by

$$\frac{dz}{\int_{l_1}^{l_2} dz}, \tag{17}$$

and the proportion of the moment of inertia of the microelement in segment $l_1 \sim l_2$ is expressed as follows:

$$\frac{I_t dz}{\int_{l_1}^{l_2} dz}. \tag{18}$$

The moment of inertia of segment $l_1 \sim l_2$ corresponds to the above integral and is expressed as follows:

$$I_2 = \frac{\int_{l_1}^{l_2} I_t dz}{\int_{l_1}^{l_2} dz} = \frac{\int_{l_1}^{l_2} f(z) dz}{\int_{l_1}^{l_2} dz}. \tag{19}$$

When segment $l_1 \sim l_2$ is discrete, as is segment q, its moment of inertia is given by

$$I_2 = \frac{\sum_{i=1}^{q} \left(\int_{l_{i-1}}^{l_i} f_i(z) dz \right)}{l_2 - l_1} = \frac{\sum_{i=1}^{q} \left(\int_{l_{i-1}}^{l_i} f_i(z) dz \right)}{L_2}, \tag{20}$$

where $f_i(z)$ is the inertia function of segment, i, l_{i-1} is the lower limit value of segment, i in the coordinate system, l_i is the upper limit value of segment i in the coordinate system, and L_2 is the length of segment $l_1 \sim l_2$.

In the above formula, the analytical expression of the moment of inertia of segment $l_1 \sim l_2$ contains an integral formula, which is not conducive to application; therefore, it can be simplified to the following expression:

$$I_2 = \frac{\sum_{i=1}^{q} z_i I_i}{\sum_{i=1}^{q} z_i}, \tag{21}$$

where q is the discrete number of segment $l_1 \sim l_2$ of the tower, I_i is the moment of inertia of segment i, and z_i is the length of segment i.

The equations for I_1 and I_3 have the same form as Equation (21). In practical engineering, the diameter and thickness of offshore wind towers change from bottom to top. The effect of this change on the structural stiffness through the moment of inertia is now considered.

(2) Solution to equivalent natural frequency problem

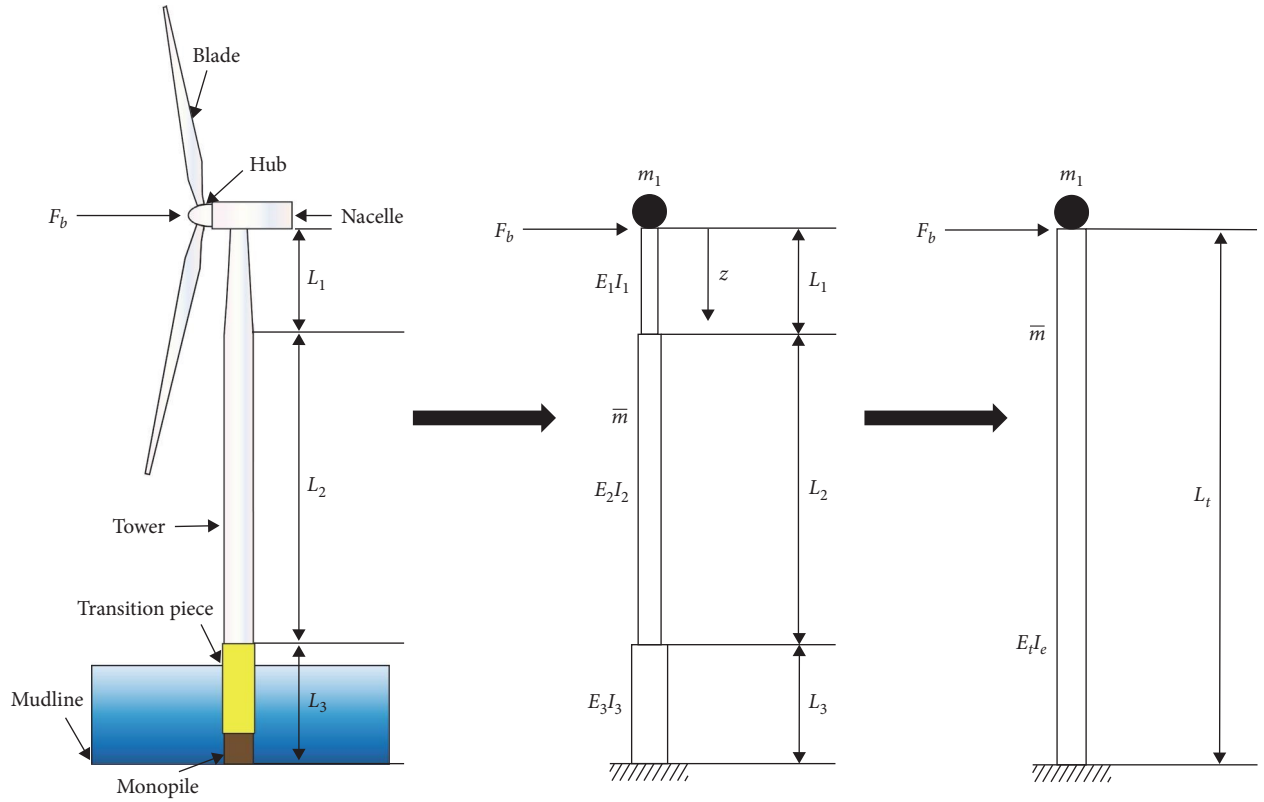

FIGURE 5: Calculation model for natural frequency without considering SSI.

In Figure 2, the moment of inertia I_t is uniform, which is an ideal model. The moment of inertia varies among the diameter-varying segment of the tower (the tapering segment), the segment with constant tower diameter or the segment with mildly varying tower diameter, the transition piece, and the monopile. To apply Equation (13) for the calculation of the natural frequency of the OWT structures with monopile foundations, the moment of inertia of the diameter-varying segment of the tower, the segment with constant tower diameter or the segment with mildly varying tower diameter, the transition piece, and the monopile, must be transformed into equivalent measures. The calculation model for the natural frequency without considering the SSI is shown in Figure 5.

According to Crotti–Engesser's theorem, the elastic displacement can be expressed as follows:

$$D_{\mathrm{F}} = \frac{\partial V_{\mathrm{C}}}{\partial F}, \tag{22}$$

where V_{C} is the complementary energy of strain and F represents forces.

Regarding the OWTs, when the wind turbine load F_{b} is applied on the hub on the tower top, the displacement at the tower top can be expressed as follows

$$\begin{aligned} D_{\mathrm{F}} &= \frac{\partial}{\partial F}\int_0^{L_1+L_2+L_3} \frac{[M(z)]^2}{2EI(z)}\,\mathrm{d}z = \frac{\partial}{\partial F}\int_0^{L_1} \frac{(F_{\mathrm{b}}z)^2}{2E_1I_1}\,\mathrm{d}z \\ &\quad + \frac{\partial}{\partial F}\int_{L_1}^{L_1+L_2} \frac{(F_{\mathrm{b}}z)^2}{2E_2I_2}\,\mathrm{d}z + \frac{\partial}{\partial F}\int_{L_1+L_2}^{L_1+L_2+L_3} \frac{(F_{\mathrm{b}}z)^2}{2E_3I_3}\,\mathrm{d}z \\ &= \frac{F_{\mathrm{b}}L_1^3}{3E_1I_1} + \frac{F_{\mathrm{b}}(L_1+L_2)^3 - F_{\mathrm{b}}L_1^3}{3E_2I_2} \\ &\quad + \frac{F_{\mathrm{b}}(L_1+L_2+L_3)^3 - F_{\mathrm{b}}(L_1+L_2)^3}{3E_3I_3}, \end{aligned} \tag{23}$$

where $M(z)$ is $F_{\mathrm{b}}z$, L_1 is the length of the diameter-varying segment of the tower, L_2 is the length of the segment with constant tower diameter or the segment with mildly varying tower diameter, L_3 is the length from the mudline to the tower bottom, E_1I_1 is the flexural stiffness of the diameter-varying segment of the tower, E_2I_2 is the flexural stiffness of the segment with constant tower diameter or the segment with mildly varying tower diameter, and E_3I_3 is the flexural stiffness from the mudline to the tower bottom.

Substituting $\frac{L_1}{L_{\mathrm{t}}} = \beta_1$, $\frac{L_2}{L_{\mathrm{t}}} = \beta_2$, and $\frac{L_3}{L_{\mathrm{t}}} = \beta_3$ into the above equation yields

$$D_F = \frac{F_b \beta_1^3 L_t^3}{3E_1 I_1} + \frac{F_b[(\beta_1+\beta_2)^3 - \beta_1^3]L_t^3}{3E_2 I_2} + \frac{F_b[1-(\beta_1+\beta_2)^3]L_t^3}{3E_3 I_3}, \tag{24}$$

and the structural displacement under unit load can be expressed as follows

$$D_1 = \frac{\beta_1^3 L_t^3}{3E_1 I_1} + \frac{[(\beta_1+\beta_2)^3 - \beta_1^3]L_t^3}{3E_2 I_2} + \frac{[1-(\beta_1+\beta_2)^3]L_t^3}{3E_3 I_3}. \tag{25}$$

According to the definition of stiffness, the structural stiffness is the reciprocal of Equation (25).

$$K = \frac{1}{D_1}. \tag{26}$$

Another structural stiffness can be expressed in the following equation:

$$K_e = \frac{3E_t I_e}{L_t^3}. \tag{27}$$

Now, we equate Equations (26) and (27). For an OWT with a monopile foundation made of steel, the elastic modulus of steel can be considered as the elastic modulus at all locations, and all the moduli are equal ($E_1 = E_2 = E_3 = E_t$). The elastic moduli at both sides of the equal sign can be reduced, yielding the following simplified equation:

$$I_e = \frac{I_1 I_2 I_3}{\beta_1^3 I_2 I_3 + [(\beta_1+\beta_2)^3 - \beta_1^3]I_1 I_3 + [1-(\beta_1+\beta_2)^3]I_1 I_2}. \tag{28}$$

If the structure above the mudline is a linearly tapered tower, I_e can be expressed as follows:

$$I_e = I_1. \tag{29}$$

The equivalent moment of inertia is introduced through the stiffness, which is approximately equal to the generalized stiffness. Therefore, the equivalent moment of inertia can be introduced through the generalized stiffness, and the equivalent mass can be introduced using the generalized mass. For a structure with one fixed support and one free end, the generalized mass [39] is expressed as follows:

$$m^* = 0.228\overline{m}L_t. \tag{30}$$

With the equivalent mass introduced through the generalized mass, the coefficient μ in Equation (11) can be corrected to

$$\mu = \frac{m_1}{0.228\overline{m}L_t}, \tag{31}$$

and Equation (13) can be corrected to

$$f_t = \frac{J^2}{2\pi}\sqrt{\frac{E_t I_e}{0.228\overline{m}L_t^4}}. \tag{32}$$

2.2. Natural Frequency with SSI. The following analysis focuses on the eigen solutions of a linear system; therefore, the nonlinear soil behavior is not modeled. The foundation systems generally do not go into a nonlinear regime, and therefore, a linear approximation is considered acceptable [10]. An OWT structure with a monopile foundation includes a nacelle, hub, blade, tower, transition piece, and monopile. The interaction between the monopile and soil below the mudline can be represented by three flexibility dimensions, as shown in Figure 6: horizontal flexibility δ_L, rotational flexibility δ_R, and coupling flexibility δ_{LR}. Generally, the settlement at the monopile foundation root is not considered; therefore, the inclined spring model is used, as shown in Figure 6.

The horizontal force and bending moment on the mudline as well as the horizontal displacement and slope on the mudline of a monopile can be expressed using the following equations:

$$\begin{Bmatrix} y_0 \\ \psi_0 \end{Bmatrix} = \begin{bmatrix} \delta_L & \delta_{LR} \\ \delta_{LR} & \delta_R \end{bmatrix} \begin{Bmatrix} F_0 \\ M_0 \end{Bmatrix}, \tag{33}$$

where F_0 is the horizontal force on the mudline, M_0 is the bending moment on the mudline, y_0 is the monopile displacement on the mudline, and ψ_0 is the monopile slope on the mudline.

With a load F_b on the tower top, the support displacement is C_R. To calculate the displacement y_t on the tower top, a virtual force system must be provided based on the virtual work principle. With a nonzero-force increment δF_b imposed on the tower top, the nonzero-force increment at the support is δF_R, as shown in Figure 7.

The increments of the bending moment M and end reaction F_R are expressed as follows:

$$\delta M = \frac{\partial M}{\partial F_b}\delta F_b, \tag{34}$$

$$\delta F_R = \frac{\partial F_R}{\partial F_b}\delta F_b. \tag{35}$$

The virtual force system performs virtual work in the deformation state, and its virtual force equation is given as follows:

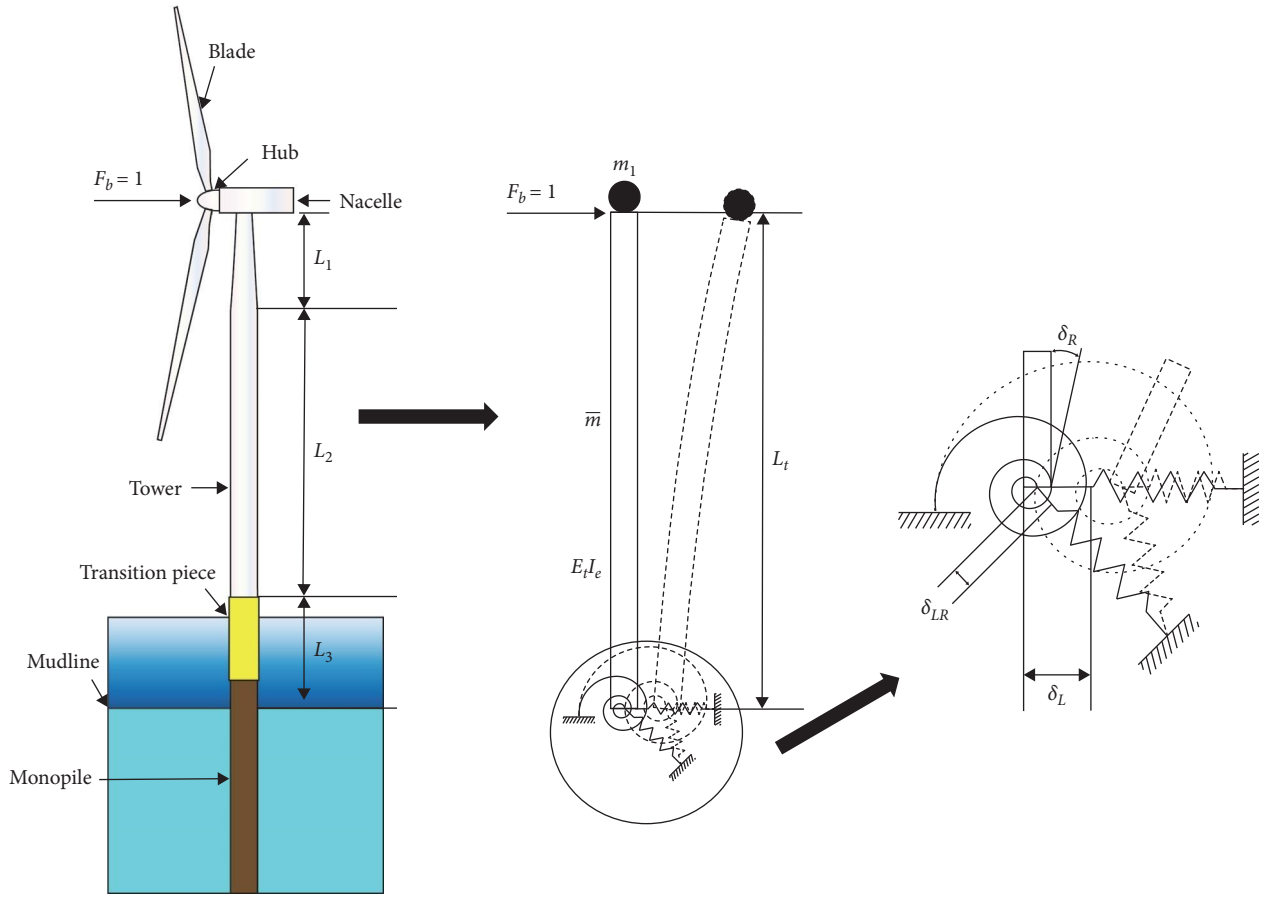

FIGURE 6: Model of an OWT with a monopile foundation.

$$y_t \delta F_b + C_R \delta F_R = \int_0^{L_t} \frac{M}{E_t I_e} \delta M dz. \tag{36}$$

Substituting Equations (34) and (35) into Equation (36) gives

$$y_t = \int_0^{L_t} \frac{M}{E_t I_e} \frac{\partial M}{\partial F_b} dz - C_R \frac{\partial F_R}{\partial F_b}. \tag{37}$$

Since the support displacement C_R and support reaction F_R are functions of F_b, this yields

$$\frac{\partial (C_R F_R)}{\partial F_b} = C_R \frac{\partial F_R}{\partial F_b} + F_R \frac{\partial C_R}{\partial F_b}. \tag{38}$$

By substituting Equation (38) into Equation (37), the following simplified equation is obtained as follows:

$$y_t = \frac{\partial}{\partial F_b} \int_0^{L_t} \frac{M^2}{2E_t I_e} dz - \frac{\partial (C_R F_R)}{\partial F_b} + F_R \frac{\partial C_R}{\partial F_b}. \tag{39}$$

The first integrand to the right of the equal sign in Equation (39) is the complementary strain energy density; therefore, Equation (39) can be expressed as follows:

$$y_t = \frac{\partial V_C}{\partial F_b} - \frac{\partial (C_R F_R)}{\partial F_b} + F_R \frac{\partial C_R}{\partial F_b}. \tag{40}$$

The support displacement C_R is given by y_0 and ψ_0, whereas the support reaction F_R is given by $-F_b$ and $-F_b L_t$. Using $F_b = F_0$ and $M_0 = F_b L_t$, the support reaction F_R can be expressed as $-F_0$ and $-M_0$. Substituting Equation (33) into Equation (40) yields

$$y_t = \frac{\partial V_C}{\partial F_b} + y_0 + \psi_0 L_t. \tag{41}$$

Figure 8 shows the deformation of the loaded tower top.

According to the deformation diagram of the loaded tower top, the total displacement of the tower top can be expressed as

$$y_t = y_0 + L_t \sin(\psi_0) + \frac{\partial V_C}{\partial F_b}. \tag{42}$$

Equations (41) and (42) are derived from the virtual work equation and geometric deformation conditions,

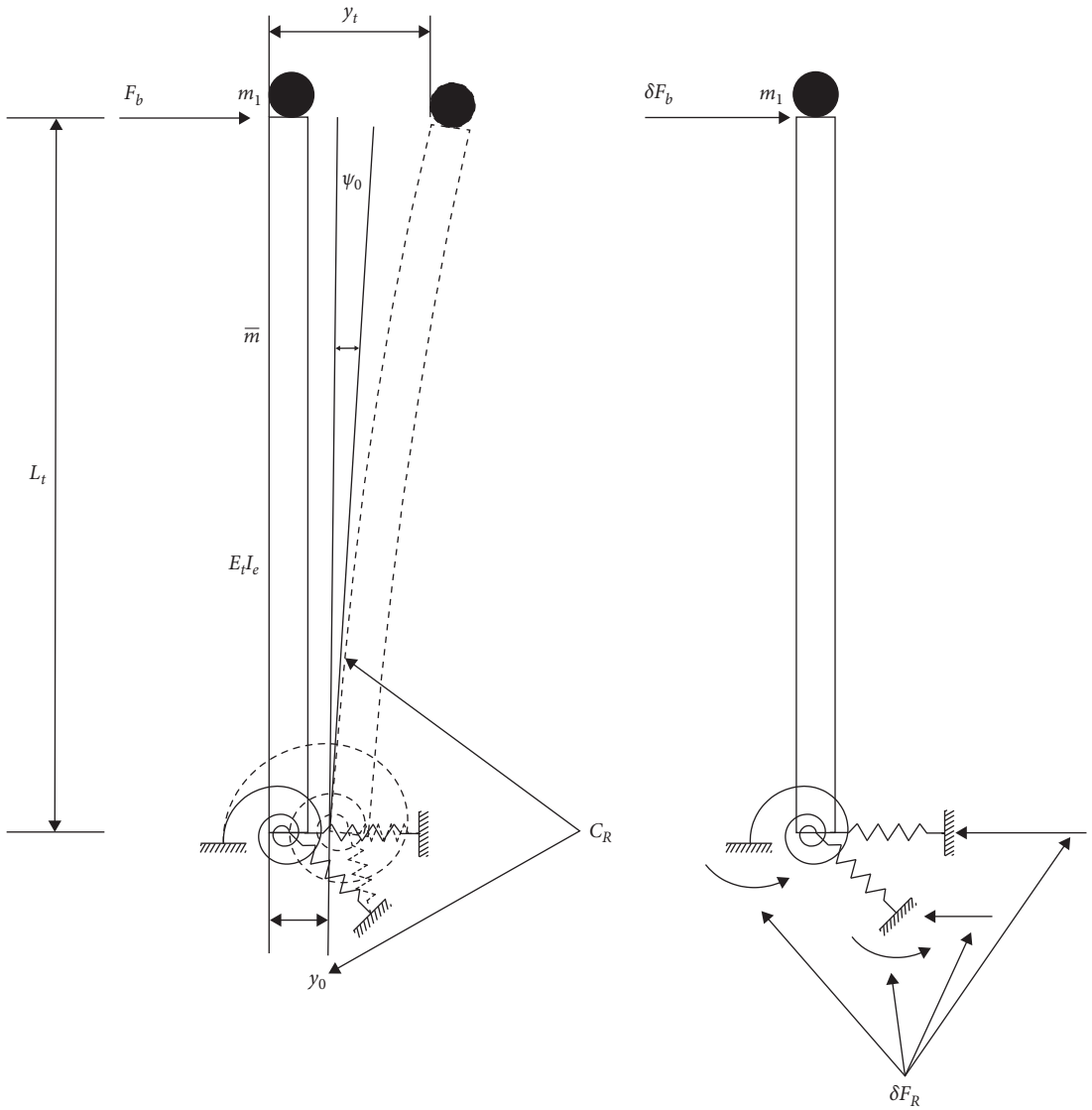

FIGURE 7: Virtual work.

respectively. With a smaller ψ_0, Equations (41) and (42) become equal according to the concept of the equivalent infinitesimal, and therefore, the two equations share the same expression. Therefore, with a smaller ψ_0, either Equations (41) or (42) can be used to represent the total displacement of the tower top after it is stressed. Equation (42) is selected to represent the total displacement at the tower top after the structural tower top is stressed.

Substituting Equation (33) into Equation (42) yields

$$y_{\mathrm{t}} = \delta_{\mathrm{L}}F_0 + \delta_{\mathrm{LR}}M_0 + L_{\mathrm{t}}\sin\left(\delta_{\mathrm{LR}}F_0 + \delta_{\mathrm{R}}M_0\right) + \frac{\partial}{\partial F_0}\int_0^{L_{\mathrm{t}}}\frac{(F_{\mathrm{b}}z)^2}{2E_{\mathrm{t}}I_{\mathrm{e}}}\mathrm{d}z. \tag{43}$$

With $M_0 = F_{\mathrm{b}}L_{\mathrm{t}}$ and $F_0 = F_{\mathrm{b}}$, Equation (43) simplifies to

$$y_{\mathrm{t}} = \delta_{\mathrm{L}}F_0 + \delta_{\mathrm{LR}}F_0L_{\mathrm{t}} + L_{\mathrm{t}}\sin\left(\delta_{\mathrm{LR}}F_0 + \delta_{\mathrm{R}}F_0L_{\mathrm{t}}\right) + \frac{F_0L_{\mathrm{t}}^3}{3E_{\mathrm{t}}I_{\mathrm{e}}}. \tag{44}$$

Considering the influence of the SSI on the natural frequency of the structure, an equivalent structure can be introduced to make the displacements at the top of the two structures equal when they are subjected to the same load. These two structures are illustrated in Figure 9.

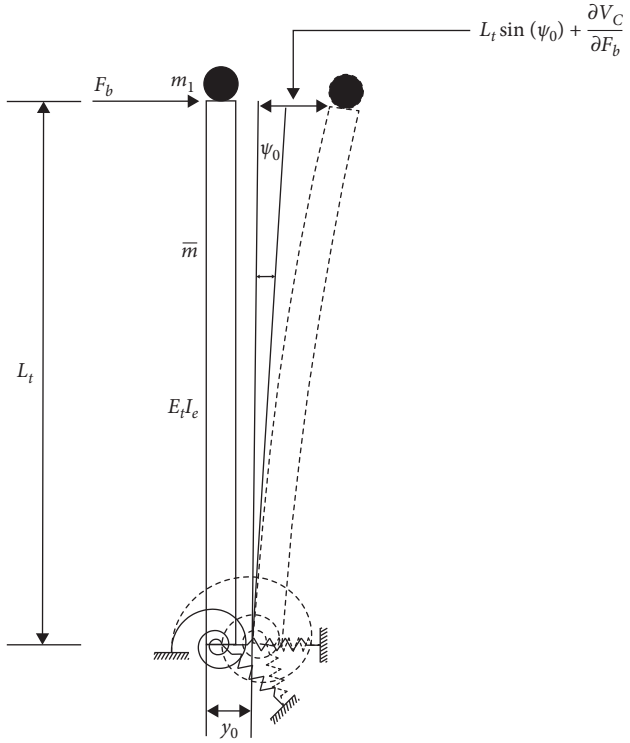

FIGURE 8: Structural deformation of the loaded tower top.

The displacement of the tower top under stress is thus expressed as follows:

$$y_t = \frac{\partial V_C}{\partial F_b} = \frac{\partial}{\partial F_b} \int_0^{L_t} \frac{(F_b z)^2}{2E_t I_s} dz = \frac{F_b L_t^3}{3E_t I_s}. \tag{45}$$

Under the same load, the top displacements of the two structures are equal:

$$\frac{F_b L_t^3}{3E_t I_s} = \delta_L F_0 + \delta_{LR} F_0 L_t + L_t \sin(\delta_{LR} F_0 + \delta_R F_0 L_t) + \frac{F_0 L_t^3}{3E_t I_e}. \tag{46}$$

Under a unit load, the displacements of both structures are equal and can be expressed as follows:

$$\frac{L_t^3}{3E_t I_s} = \delta_L + \delta_{LR} L_t + L_t \sin(\delta_{LR} + \delta_R L_t) + \frac{L_t^3}{3E_t I_e}. \tag{47}$$

After converting the numerator and denominator at both sides of the equal sign in Equation (47), the equation remains valid. At this time, both sides of the equal sign represent the structural stiffness and can be further simplified as

$$E_t I_s = \frac{L_t^3}{3\left[\delta_L + \delta_{LR} L_t + L_t \sin(\delta_{LR} + \delta_R L_t) + \frac{L_t^3}{3E_t I_e}\right]}. \tag{48}$$

The calculation equation of the structural natural frequency after considering the SSI is

$$f_s = \frac{J^2}{2\pi} \sqrt{\frac{E_t I_s}{0.228 \overline{m} L_t^4}}. \tag{49}$$

The symbol explanations are given in Table 1. Elements δ_L, δ_{LR} and δ_R of the flexibility matrix are given in Appendix A.

The natural frequency of an OWT structure with a monopile foundation considering the SSI is then calculated using the following four steps:

(1) Calculate the moment of inertia I_e above the mudline for the structure.

(2) Determine whether the monopile is rigid or slender. Depending on the soil properties, determine whether the monopile is rigid or slender using Equations (A3), (A4), (A8), and (A9). For a multilayer soil, this can be determined based on the percentage of the total thickness of the cohesive soil and the total thickness of the cohesionless soil in the embedded length of the monopile.

(3) Calculate the flexibility matrix. According to the soil properties and depending on whether the monopile is rigid or slender, calculate the flexibility matrix using Equations (A5), (A6), (A10), and (A11).

(4) Determine the natural frequency of the structure. First, substitute the elements in the flexibility matrix into Equation (48) to calculate the equivalent moment of inertia I_s. Second, substitute the equivalent moment of inertia into Equation (49) to obtain the natural frequency of the structure.

3. Simulation Comparison

3.1. Parameter Selection for a Finite Element Model. Three finite element models are employed to enable differentiation and diversity of the study objects. In each case, the following assumptions are made: the total mass m_1 of the blade, hub, and nacelle is 243,000 kg. The values of L_1, L_2, and L_3 are 35.877, 39.833, and L_3 19 m, respectively. The monopile length is 74 m, and the monopile embedded length is 55 m. Poisson's ratio is 0.3, Young's modulus is 206 Gpa, and the density is 7,850 kg/m^3. For Model 1, the outer diameter of the monopile is 5 m, and the wall thickness of the monopile is 0.06 m. For Model 2, the outer diameter of the monopile is 5.5 m, and the wall thickness of the monopile is 0.06 m. For Model 3, the outer diameter of the monopile is 5 m, and the wall thickness of the monopile is 0.08 m. The parameters of the upper tower section of the OWT are shown in Figure 10. Finite element models are shown in Figure 11. For the soil model, a hardened soil with a small-strain stiffness is employed. The parameters for the hardened soil with small-strain stiffness are given in Table 2.

In the finite element models, it is necessary to increase the elastic modulus and gravity density of the soil to reduce the horizontal displacement of the structural mudline. Using Model 1 as an example, the calculation results are shown in Figure 12.

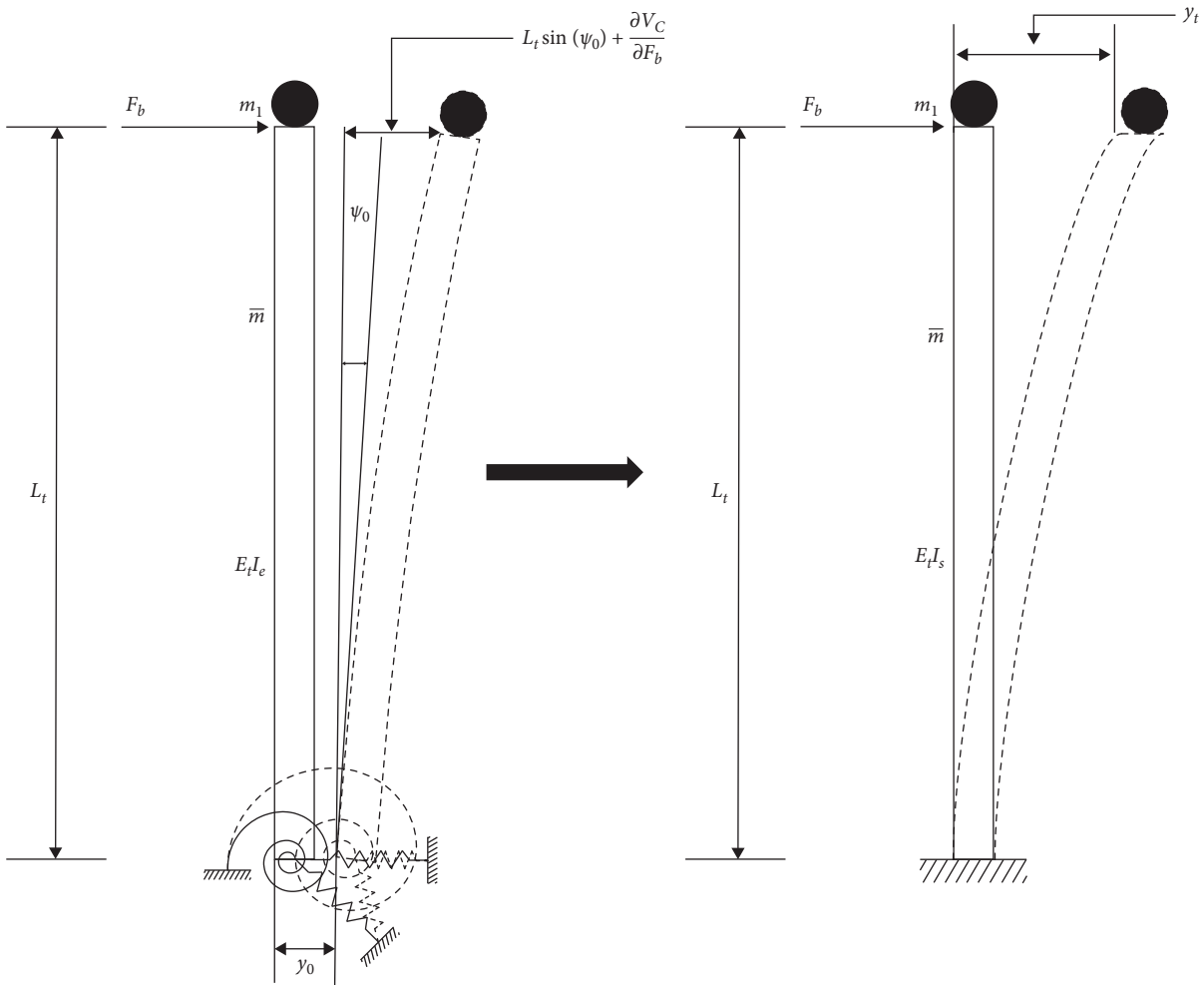

Figure 9: Equivalent structure model.

Table 1: List of symbols.

Symbol	Explanation	Symbol	Explanation
$\overline{m}$	Mass per unit length	F_b	Wind turbine load
E_t	Elastic modulus of the structure	K	Structural stiffness
I_t	Moment of inertia	K_e	Equivalent stiffness of the structure
t	Time	I_e	Equivalent moment of inertia after considering the nonuniform moment of inertia
z	Space coordinate	m^*	Generalized mass
a	Constant	f_t	Natural Frequency after considering the nonuniform moment of inertia
ω	Circular frequency	δ_L	Horizontal flexibility
$v(z,t)$	Displacement function	δ_R	Rotational flexibility
$X(z)$	Shape function	δ_{LR}	Coupling flexibility
$Y(t)$	Amplitude function	F_0	Horizontal force on the mudline
$A_1A_2A_3A_4$	Real constant	M_0	Bending moment on the mudline
L_t	Length from the mudline to the tower top	y_0	Monopile displacement on the mudline
μ	Mass ratio	ψ_0	Monopile slope on the mudline
J	Constant a times L_t	C_R	Support displacement
f	Natural frequency of OWT structures with monopile foundations	y_t	Displacement of the tower top
D	Outer diameter	F_R	End reaction

Table 1: Continued.

Symbol	Explanation	Symbol	Explanation
d_n	Inner diameter	M	Bending moment
L_1	Length of the diameter-varying segment of the tower	I_S	Equivalent moment of inertia after considering the SSI
L_2	Length of the segment with constant tower diameter or the segment with mildly varying tower diameter	f_s	Natural Frequency after considering the SSI
L_3	Length from the mudline to the tower bottom	k_h	Modulus of the subgrade reaction
I_1	Moment of inertia within a length range of L_1	D_P	Pile diameter
I_2	Moment of inertia within a length range of L_2	E	Elastic modulus of the soil
I_3	Moment of inertia within a length range of L_3	I_P	Moment of inertia of the pile
V_C	Complementary strain energy	υ_S	Poisson's ratio of the soil
$E_1E_2E_3$	Elastic modulus	β	Slenderness parameter
F	Forces	L_P	Embedded length of the pile
β_1	L_1 divided by L_t	n_h	Coefficient of the subgrade reaction
β_2	L_2 divided by L_t	z_s	Depth below the mudline
β_3	L_3 divided by L_t	E_P	Elastic modulus of the pile

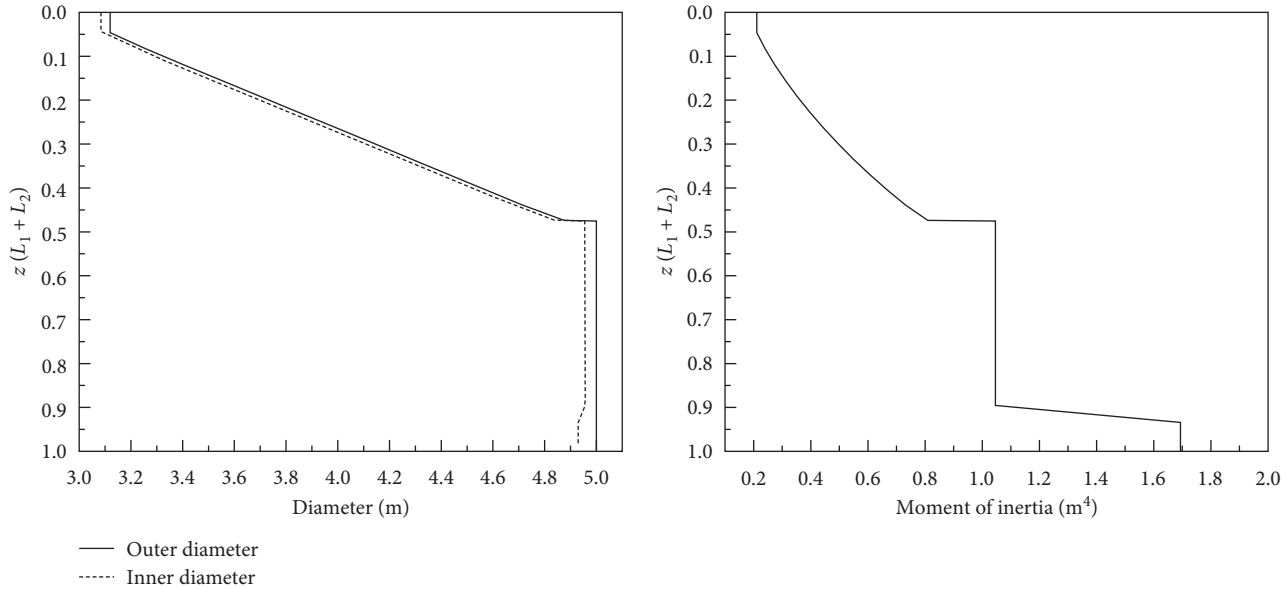

Figure 10: Parameters for the upper tower section of a 4 MW OWT.

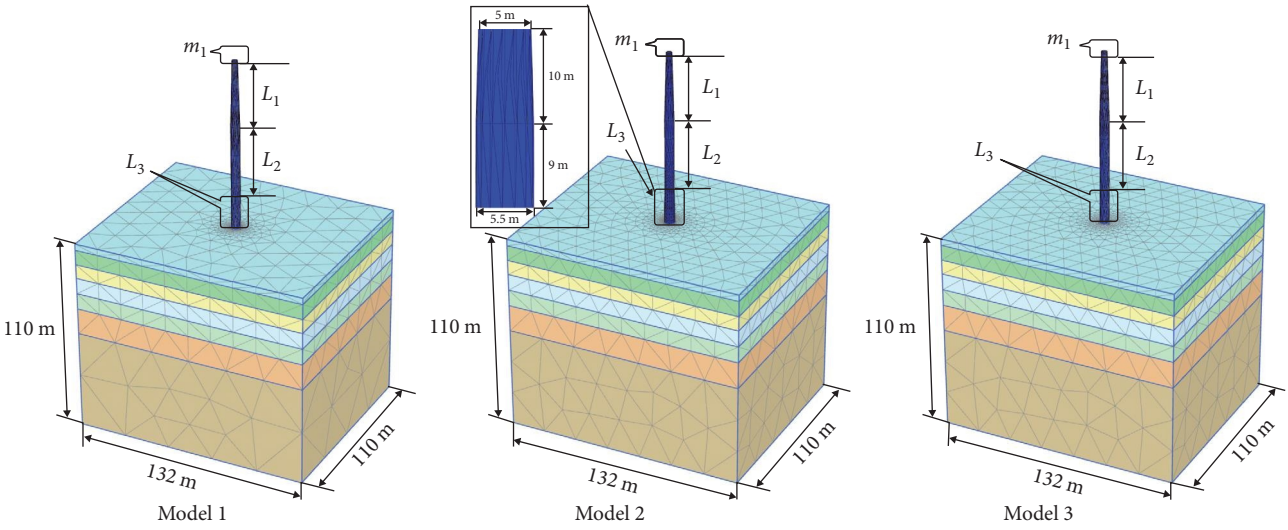

Figure 11: Finite element models.

Table 2: Parameters for hardened soil with small-strain stiffness.

Soil	Thickness/m	c/kPa	φ/°	E/MPa	$\gamma_{0.7}$	e	m	E_{50}^{ref}/MPa	E_{oed}^{ref}/MPa	E_{ur}^{ref}/MPa	G_0^{ref}/MPa
Clay	3.6	15	8.4	2.74	0.0001	1.23	0.80	4.56	3.04	24.32	44.80
Clay	8.6	15	8.4	2.68	0.0001	1.26	0.80	4.47	2.98	23.84	42.70
Silt	8.1	18	26.4	10.59	0.0001	0.72	0.60	11.80	11.80	50.03	96.84
Sand	9.2	7	33.4	16.34	0.0001	0.63	0.55	18.20	18.20	54.60	111.00
Silt	9.2	22	12.1	4.03	0.0001	0.97	0.80	5.60	4.48	29.21	67.00
Clay	15	37	17.8	5.48	0.0001	0.77	0.80	6.09	6.09	30.45	90.24
Sand	56.3	7	33.6	14.84	0.0001	0.66	0.55	16.50	16.50	54.45	106.08

$\gamma_{0.7}$ is generally 0.0001 as the threshold shear strain. e is the void ratio. m is the power for stress-level dependency of stiffness, with a value between 0.5 and 1. Sand and silt are near 0.5, and soft clay is near 1. E_{50}^{ref} is the secant stiffness in standard drained triaxial test. E_{oed}^{ref} is the tangent stiffness for primary oedometer loading. E_{ur}^{ref} is the unloading/reloading stiffness. G_0^{ref} is the shear modulus at the small strain. The un-/reloading Poisson's ratio is 0.2.

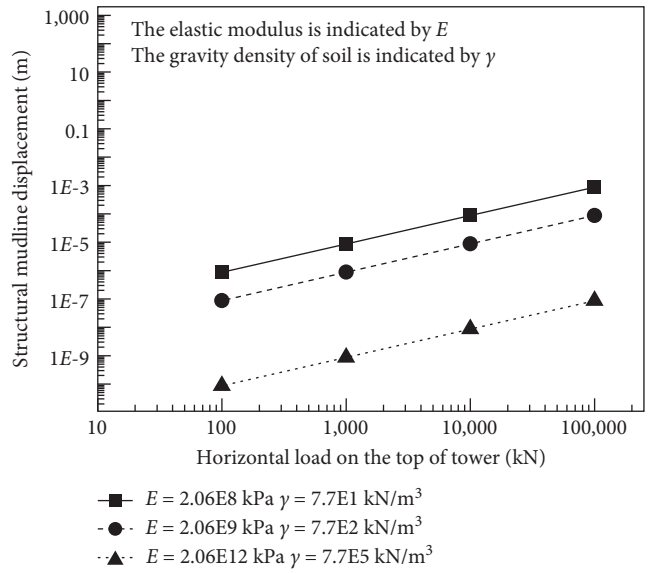

Figure 12: Displacement under different elastic moduli and gravity densities of soil.

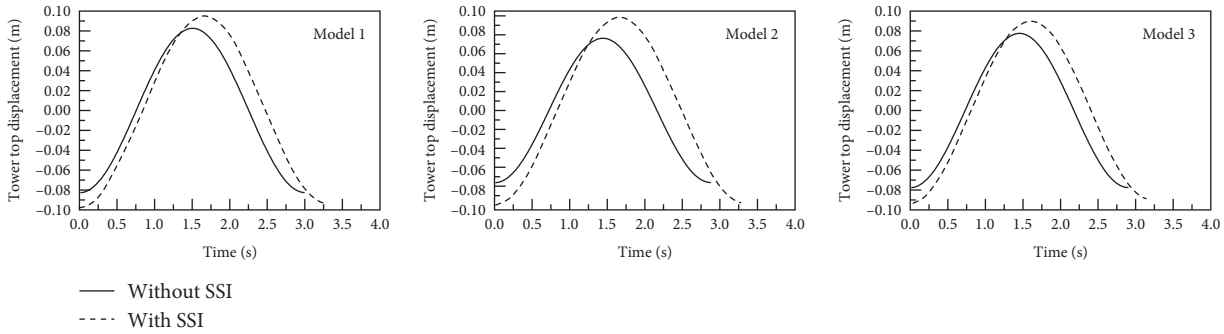

Figure 13: Cycles of the models.

As shown in Figure 12, with a gravity density of soil of 7.7E5 kN/m^3 and elastic modulus of 2.06E12 kPa, the horizontal displacement of the structural mudline is quite small, close to zero. At that time, the position of the mudline is similar to that of a fixed support; therefore, the SSI is ignored. In the following finite element calculation, the elastic modulus and gravity density of the soil are 2.06E12 kPa and 7.7E5 kN/m^3, respectively, without considering the SSI.

3.2. Comparative Analysis of Calculation Results. A horizontal load is applied to the tower top in the model, which is later removed to allow the structure to vibrate freely. The calculation results are shown Figure 13. The natural frequency of the structure can be obtained by evaluating the time required for each cycle.

According to Table 2, the total thickness of the sandy soil layer is 10.5 m, accounting for only 19.091% of the embedded

Table 3: Natural frequencies of the models.

Model	Method	Natural frequency without SSI (Hz)	Deviation (%)	Natural frequency with SSI (Hz)	Deviation (%)
1	Ko [38]	0.295	11.940	0.286	6.230
	Yang [40]	0.258	22.985	0.257	15.738
	Arany et al. [10]	0.248	25.970	0.226	25.902
	Method herein	0.323	3.582	0.304	0.328
	Finite element method	0.335	–	0.305	–
2	Ko [38]	0.305	12.104	0.295	2.318
	Yang [40]	0.291	16.138	0.290	3.974
	Arany et al. [10]	0.253	27.089	0.231	23.510
	Method herein	0.331	4.611	0.310	−2.649
	Finite element method	0.347	–	0.302	–
3	Ko [38]	0.304	12.392	0.294	6.369
	Yang [40]	0.272	21.614	0.271	13.694
	Arany et al. [10]	0.253	27.089	0.230	26.752
	Method herein	0.332	4.323	0.311	0.955
	Finite element method	0.347	–	0.314	–

length of the monopile (55 m), whereas the total thickness of the cohesive soil layer is 44.5 m, accounting for 80.909% of the embedded length of the monopile (55 m). Therefore, whether the monopile is rigid or slender is determined by the cohesive soil. According to Equations (A3) and (A4), the monopile embedded lengths in the three models are closer to the determination value of the rigid pile in Equation (A4); therefore, the monopiles in the three models are considered as rigid piles. For the layered soil, the element value in the flexibility matrix in Equation (48) is the weighted average value. To determine this, the elements in the flexibility matrix of each layer are first calculated, then multiplied by the thickness of the soil layer, and finally superimposed and divided by the monopile embedded length. The calculation results are shown in Table 3.

Different methods are used to calculate the natural frequency of the finite element model, which will be compared with the finite element calculation results. The calculation results are listed in Table 3.

According to Table 3, the calculation method for the natural frequency of the OWT structures with monopile foundations considering the SSI can consider the nonuniform moment of inertia above the mudline of the structure and the SSI into account when calculating the natural frequency of the structure. The natural frequencies of the three models are calculated and compared with the finite element results to validate this method. As shown in Table 3, the natural frequencies of the models are reduced after considering the SSI.

Compared with the calculation results of the finite elements model, the calculation results for the three models using the method proposed by Arany [10] are significantly different, with deviations ranging from 23.510% to 27.089%. The calculation results for the three models using the method proposed by Yang [40] are also significantly different, with deviations ranging from 3.974% to 22.985%. The reason for the significant deviation in the calculation results of the two methods is that the three models are beyond the scope of application of both approaches. Compared with the calculation results from the finite element model, the calculation results for the three models using the method proposed by Ko [38] are different, with deviations ranging from 2.318% to 12.392%.

To investigate the effect of μ on the frequency, only the mass of m_1 in Models 1, 2, and 3 is changed. In Figures 14–17, the coefficient μ in Equation (11) is employed.

The natural frequency decreases as μ increases. The deviation between the finite element calculation results and the calculation results of the simplified method is small, indicating that the simplified method used in this study meets the engineering accuracy requirement.

3.3. Other Simulation Comparison. The OWT parameters are obtained from relevant literature [41]. The bottom of the tower is fixed. The structure above the mudline is only a tapered tower; thus, Equation (29) is used to calculate I_e. The calculation results are listed in Table 4.

According to the comparison of the calculation results between the four natural-frequency simplified calculation methods and the numerical calculation, the difference between the Arany method and the numerical calculation is large, indicating that the model with such geometric features is beyond the scope of application of the Arany method.

The OWT parameters are obtained from relevant literature [42]. It should be noted that the 1P range for the 10 MW DTU corresponds to 0.1–0.16 Hz, whereas the 3P range corresponds to 0.3–0.48 Hz [43]. Considering a safety margin of 10%, the "allowable" frequency range for the OWT is thus 0.176–0.273 Hz [42]. The calculation results are listed in Table 5.

Without considering the SSI, the calculation results of the Yang and Arany methods are significantly different from the finite element calculation results. This difference is significantly reduced when the SSI is considered. This is because the finite element calculation results considering the SSI are reduced by 11.106% compared with the finite element

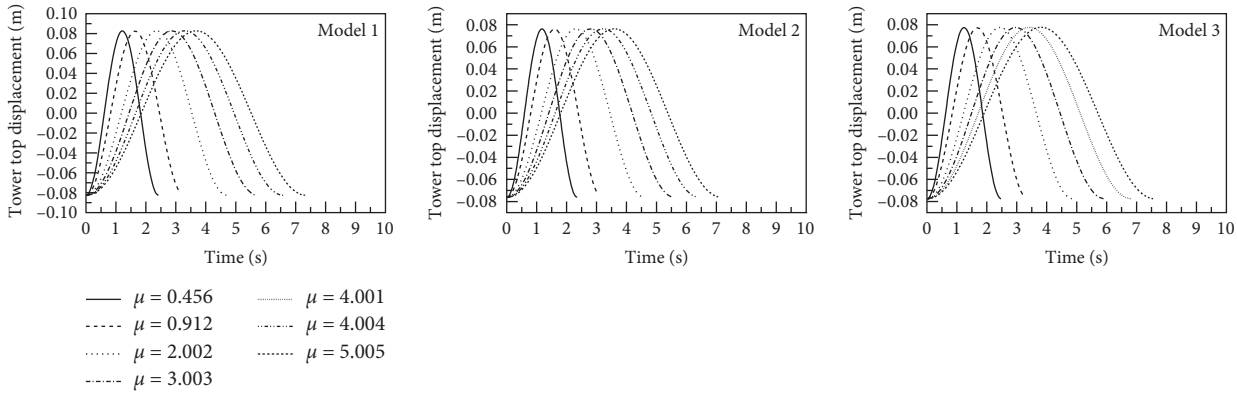

Figure 14: Cycles of the models without SSI.

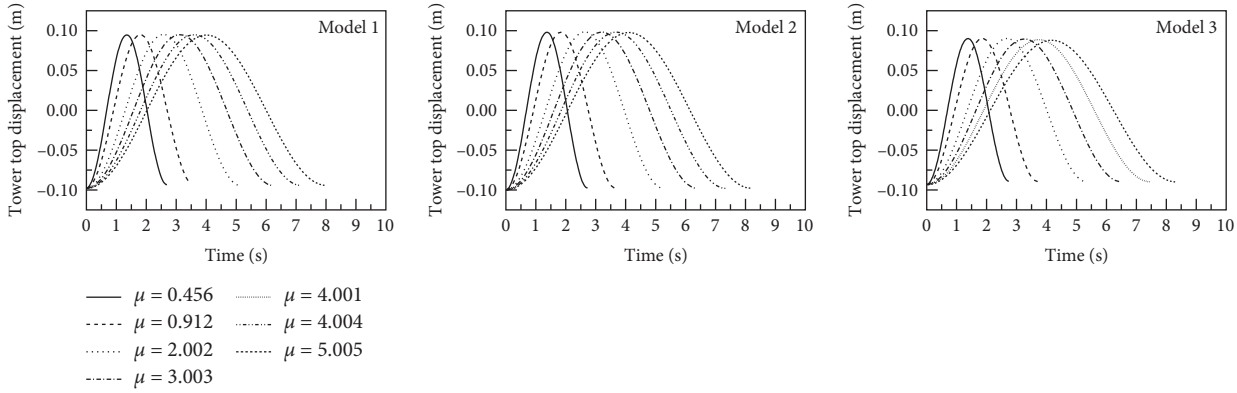

Figure 15: Cycles of the models with SSI.

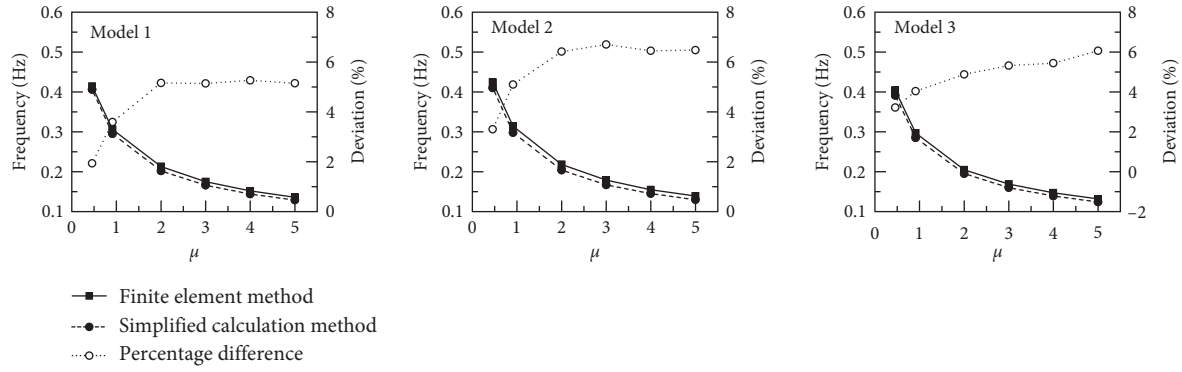

Figure 16: Natural frequency comparison without considering the SSI.

calculation results without the SSI, and the single-digit percentage is reduced by other methods. The results of the four simplified calculation methods are within the allowable range.

Whether or not the SSI is considered, the simplified calculation method proposed in this paper performs well for tapered and multisegment towers. Therefore, this simplified calculation method has a wide range of applications.

When the SSI is not considered, Ko's method performs well for tapered towers. It is worth noting that there are errors in Equations (11) and (15) in Ko's paper [38] and that the method can only be used after modifying the formulas. The Ko calculation method is suitable for models with tapered towers and substructures above the mudline and for models with only a tapered tower above the mudline. This method considers the changes in the moment of inertia and mass of the tapered tower.

In the Yang calculation method, it is assumed that the tower wall thickness is constant and the structure above the mudline is a tapered tower. Therefore, this method is suitable for models with only a tapered tower above the mudline.

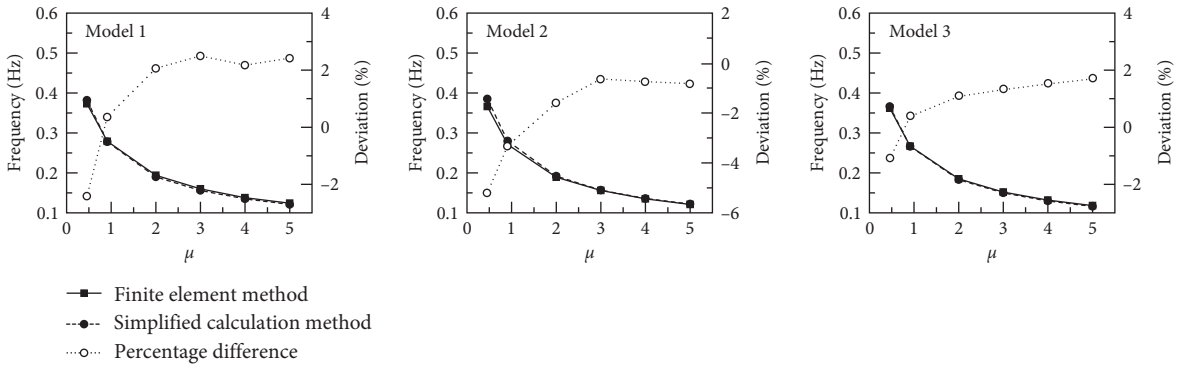

Figure 17: Natural frequency comparison considering the SSI.

Table 4: Comparison of natural frequencies calculated using various methods.

Method	Natural frequency (Hz)	Deviation (%)	Deviation (%)
Ko [38]	0.3243	−0.0926	−1.502
Yang [40]	0.3321	−2.500	−3.944
Arany et al. [10]	0.2788	13.951	12.739
Method herein	0.3115	3.858	2.504
ADAMS Jonkman et al. [41]	0.3195	1.389	–
FAST Jonkman et al. [41]	0.3240	–	−1.408

Table 5: Comparison of natural frequencies calculated using various methods.

Method	Natural frequency without SSI (Hz)	Deviation (%)	Natural frequency with SSI (Hz)	Deviation (%)	Deviation (%)
Ko [38]	0.228	−0.885	0.2271	−13.041	0.395
Yang [40]	0.192	15.044	0.1874	6.720	2.396
Arany et al. [10]	0.206	8.850	0.1981	1.394	3.835
Method herein	0.221	2.212	0.2176	−8.313	1.538
Alkhoury et al. [42]	0.226	–	0.2009	–	11.106

In the Arany calculation method, it is assumed that a tapered tower with a variable wall thickness is ideally equivalent to a tower with a constant diameter and wall thickness and that the structure above the mudline comprises a tapered tower and substructure (monopile and transition piece). Therefore, this method is suitable for models with tapered towers and substructures above the mudline.

4. Conclusion

Based on the Euler–Bernoulli beam theory, an approximation algorithm was proposed to determine the natural frequencies of the OWT structures with monopile foundations. The algorithm considers the effects of changes in the diameter and wall thickness of the structure above the mudline on the natural frequency, using segmentation and a weighted average. The effect of the soil around the monopile on the natural frequency is also considered. Unlike existing numerical methods, this algorithm does not require programing. Compared with other approximation algorithms for the natural frequencies of the OWT structures with monopile foundations, the algorithm can consider not only the impact of the structural wall thickness changes on the natural frequency but also the impact of more complex cross-sectional changes; thus, the algorithm provides more accurate calculations and can be applied more widely.

Moreover, a coefficient μ was introduced to consider the influence of the changes in the lumped mass on the tower top and in the total mass of the tower, the transition piece, and the monopile above the mudline of the structure on the natural frequency. By solving the transcendental Equation (11), the relationship between μ and J can be established.

In addition, two finite element calculation models were established: without and with consideration of the SSI. According to the finite element calculations, the natural frequency calculated using the former model is higher than that calculated using the latter. In the calculation using the model without considering the SSI, it was found that the natural frequency of the OWT structure is overestimated because the model does not adequately include the displacement and slope of the position of the monopile mudline.

Appendix

A. Flexibility matrix

The calculation method for the flexibility matrix of rigid and slender piles is provided by Poulos and Davis [44] based on the constant or linear modulus of the subgrade reaction k_h.

(1) Cohesive soil

The modulus of the subgrade reaction k_h of the cohesive soil is a constant, which is calculated as follows [45]:

$$k_h = \frac{0.65}{D_P}\sqrt[12]{\frac{ED_P^4}{E_P I_P}}\left(\frac{E}{1-\upsilon_S^2}\right), \tag{A1}$$

where D_P is the pile diameter, E is the elastic modulus of the soil, E_P is the elastic modulus of the pile, I_P is the moment of inertia of the pile, and υ_S is Poisson's ratio of the soil.

The calculation method for the slenderness parameter β, is provided by Poulos and Davis [44].

$$\beta = \sqrt[4]{\frac{k_h D_P}{4E_P I_P}}. \tag{A2}$$

(2) Slender and rigid piles in cohesive soils

Poulos and Davis [44] proposed a determination method for slender and rigid piles under the condition of constant modulus of subgrade reaction.

(a) Slender piles

$$L_P > 2.5\left(\frac{4E_P I_P}{k_h D_P}\right)^{1/4}, \tag{A3}$$

where L_P is the embedded length of the pile.

(b) Rigid piles

$$L_P < 1.5\left(\frac{4E_P I_P}{k_h D_P}\right)^{1/4}. \tag{A4}$$

(3) Stiffness matrix of cohesive soil

The displacement and slope equations of slender piles under the condition of constant modulus of subgrade reaction are expressed in Equation (A5), as proposed by Poulos and Davis [44].

$$\begin{Bmatrix} y_0 \\ \psi_0 \end{Bmatrix} = \begin{bmatrix} \frac{2\beta}{k_h D_P} & \frac{2\beta^2}{k_h D_P} \\ \frac{2\beta^2}{k_h D_P} & \frac{4\beta^3}{k_h D_P} \end{bmatrix} \begin{Bmatrix} F_0 \\ M_0 \end{Bmatrix}, \tag{A5}$$

where β is the slenderness parameter.

The displacement and slope equations for rigid piles under the condition of constant modulus of the subgrade reaction are expressed in Equation (A6), as proposed by Poulos and Davis [44].

$$\begin{Bmatrix} y_0 \\ \psi_0 \end{Bmatrix} = \begin{bmatrix} \frac{4}{k_h D_P L_P} & \frac{6}{k_h D_P L_P^2} \\ \frac{6}{k_h D_P L_P^2} & \frac{12}{k_h D_P L_P^3} \end{bmatrix} \begin{Bmatrix} F_0 \\ M_0 \end{Bmatrix}. \tag{A6}$$

(4) Noncohesive soil

The noncohesive soil modulus of subgrade reaction k_h is linear, and it is calculated as follows [44]:

$$k_h = n_h \cdot \frac{z_s}{D_p}, \tag{A7}$$

where n_h is the coefficient of the subgrade reaction and z_s is the depth below the mudline.

(5) Slender and rigid piles in noncohesive soil

Poulos and Davis [44] proposed a determination method for slender and rigid piles under the condition of linear modulus of subgrade reaction.

(a) Slender pile

$$L_P > 4.0\left(\frac{E_P I_P}{n_h}\right)^{1/5}. \tag{A8}$$

(b) Rigid pile

$$L_P < 2.0\left(\frac{E_P I_P}{n_h}\right)^{1/5}. \tag{A9}$$

(6) Stiffness matrix in noncohesive soil

The displacement and slope equations of a slender pile under the condition of linear modulus of subgrade reaction are expressed in Equation (A10), as proposed by Poulos and Davis [44].

$$\begin{Bmatrix} y_0 \\ \psi_0 \end{Bmatrix} = \begin{bmatrix} \frac{2.40}{n_h^{3/5}(E_P I_P)^{2/5}} & \frac{1.60}{n_h^{2/5}(E_P I_P)^{3/5}} \\ \frac{1.60}{n_h^{2/5}(E_P I_P)^{3/5}} & \frac{1.74}{n_h^{1/5}(E_P I_P)^{4/5}} \end{bmatrix} \begin{Bmatrix} F_0 \\ M_0 \end{Bmatrix}. \tag{A10}$$

The displacement and slope equations of a rigid pile under the condition of linear modulus of the subgrade reaction are expressed in Equation (A11), as proposed by Poulos and Davis [44].

$$\begin{Bmatrix} y_0 \\ \psi_0 \end{Bmatrix} = \begin{bmatrix} \dfrac{18}{L_P^2 n_h} & \dfrac{23.94}{L_P^3 n_h} \\ \dfrac{24}{L_P^3 n_h} & \dfrac{36}{L_P^4 n_h} \end{bmatrix} \begin{Bmatrix} F_0 \\ M_0 \end{Bmatrix}. \quad \text{(A11)}$$

Data Availability

The authors confirm that the data supporting the findings of this study are available within the article.

Conflicts of Interest

The authors declare that they have no conflicts of interest.

Acknowledgments

National Natural Science Foundation of China funded project (5167082378).

References

[1] S. Darvishi-Alamouti, M.-R. Bahaari, and M. Moradi, "Natural frequency of offshore wind turbines on rigid and flexible monopiles in cohesionless soils with linear stiffness distribution," *Applied Ocean Research*, vol. 68, pp. 91–102, 2017.

[2] I. Depina, T. M. Hue Le, G. Eiksund, and T. Benz, "Behavior of cyclically loaded monopile foundations for offshore wind turbines in heterogeneous sands," *Computers and Geotechnics*, vol. 65, pp. 266–277, 2015.

[3] S. Corciulo, O. Zanoli, and F. Pisanò, "Transient response of offshore wind turbines on monopiles in sand: role of cyclic hydro–mechanical soil behaviour," *Computers and Geotechnics*, vol. 83, pp. 221–238, 2017.

[4] S.-P. Breton and G. Moe, "Status, plans and technologies for offshore wind turbines in Europe and North America," *Renewable Energy*, vol. 34, no. 3, pp. 646–654, 2009.

[5] G. M. Álamo, J. J. Aznárez, L. A. Padrón, A. E. Martínez-Castro, R. Gallego, and O. Maeso, "Dynamic soil–structure interaction in offshore wind turbines on monopiles in layered seabed based on real data," *Ocean Engineering*, vol. 156, pp. 14–24, 2018.

[6] R. Harrabin, *Offshore Wind Power Cheaper than New Nuclear 2017*, BBC, 2017.

[7] Wind Europe, "The european offshore wind industry," in *Key Trends and Statistics 2017*, p. 37, Wind Europe, Brussels, Belgium, 2018.

[8] D. Lombardi, S. Bhattacharya, and D. Muir Wood, "Dynamic soil–structure interaction of monopile supported wind turbines in cohesive soil," *Soil Dynamics and Earthquake Engineering*, vol. 49, pp. 165–180, 2013.

[9] M. Karimirad, *Offshore Energy Structures For Wind Power, Wave Energy and Hybrid Marine Platforms*, Springer International Publishing, Switzerland, 2014.

[10] L. Arany, S. Bhattacharya, J. H. G. Macdonald, and S. J. Hogan, "Closed form solution of eigen frequency of monopile supported offshore wind turbines in deeper waters incorporating stiffness of substructure and SSI," *Soil Dynamics and Earthquake Engineering*, vol. 83, pp. 18–32, 2016.

[11] J. van der Tempel and D.-P. Molenaar, "Wind turbine structural dynamics—a review of the principles for modern power generation, onshore and offshore," *Wind Engineering*, vol. 26, no. 4, pp. 211–222, 2002.

[12] S. Bhattacharya, J. A. Cox, D. Lombardi, and D. Muir Wood, "Dynamics of offshore wind turbines supported on two foundations," *Proceedings of the Institution of Civil Engineers - Geotechnical Engineering*, vol. 166, no. 2, pp. 159–169, 2013.

[13] F. Petrini, H. Li, and F. Bontempi, "Basis of design and numerical modeling of offshore wind turbines," *Structural Engineering and Mechanics*, vol. 36, no. 5, pp. 599–624, 2010.

[14] G. Bertollucci Colherinhas, F. Petrini, M. V. G. de Morais, and F. Bontempi, "Optimal design of passive-adaptive pendulum tuned mass damper for the global vibration control of offshore wind turbines," *Wind Energy*, vol. 24, no. 6, pp. 573–595, 2021.

[15] V. Laface, G. Alotta, G. Failla, C. Ruzzo, and F. Arena, "A two-degree-of-freedom tuned mass damper for offshore wind turbines on floating spar supports," *Marine Structures*, vol. 83, Article ID 103146, 2022.

[16] G. Alotta, C. Biondo, A. Giaralis, and G. Failla, "Seismic protection of land-based wind turbine towers using the tuned inerter damper," *Structures*, vol. 51, pp. 640–656, 2023.

[17] V. Jahangiri and C. Sun, "A novel three dimensional nonlinear tuned mass damper and its application in floating offshore wind turbines," *Ocean Engineering*, vol. 250, Article ID 110703, 2022.

[18] S. Xie, X. Jin, J. He, J. Gao, C. Zhang, and Y. Yan, "Applying multiple tuned mass dampers to control structural loads of bottom-fixed offshore wind turbines with inclusion of soil–structure interaction," *Ocean Engineering*, vol. 205, Article ID 107289, 2020.

[19] C. Sun and V. Jahangiri, "Bi-directional vibration control of offshore wind turbines using a 3D pendulum tuned mass damper," *Mechanical Systems and Signal Processing*, vol. 105, pp. 338–360, 2018.

[20] J. Yang, E. M. He, and Y. Q. Hu, "Dynamic modeling and vibration suppression for an offshore wind turbine with a tuned mass damper in floating platform," *Applied Ocean Research*, vol. 83, pp. 21–29, 2019.

[21] B. Fitzgerald, J. McAuliffe, S. Baisthakur, and S. Sarkar, "Enhancing the reliability of floating offshore wind turbine towers subjected to misaligned wind–wave loading using tuned mass damper inerters (TMDIs)," *Renewable Energy*, vol. 211, pp. 522–538, 2023.

[22] Z. Zhang and C. Høeg, "Inerter-enhanced tuned mass damper for vibration damping of floating offshore wind turbines," *Ocean Engineering*, vol. 223, Article ID 108663, 2021.

[23] H. Ding, O. Altay, and J.-T. Wang, "Lateral vibration control of monopile supported offshore wind turbines with toroidal tuned liquid column dampers," *Engineering Structures*, vol. 286, Article ID 116107, 2023.

[24] X. Liu, J. Xu, G. He, and C. Chen, "Lateral vibration mitigation of monopile offshore wind turbines with a spring pendulum pounding tuned mass damper," *Ocean Engineering*, vol. 266, Part 4, Article ID 112954, 2022.

[25] M. Hussan, M. S. Rahman, F. Sharmin, D. Kim, and J. Do, "Multiple tuned mass damper for multi-mode vibration reduction of offshore wind turbine under seismic excitation," *Ocean Engineering*, vol. 160, pp. 449–460, 2018.

[26] D. Chen, S. Huang, C. Huang, R. Liu, and F. Ouyang, "Passive control of jacket-type offshore wind turbine vibrations by single and multiple tuned mass dampers," *Marine Structures*, vol. 77, Article ID 102938, 2021.

[27] G. M. Stewart and M. A. Lackner, "The impact of passive tuned mass dampers and wind–wave misalignment on

offshore wind turbine loads," *Engineering Structures*, vol. 73, pp. 54–61, 2014.

[28] J. W. Zhang, X. Liang, L. Z. Wang, B. X. Wang, and L. L. Wang, "The influence of tuned mass dampers on vibration control of monopile offshore wind turbines under wind–wave loadings," *Ocean Engineering*, vol. 278, Article ID 114394, 2023.

[29] V. Jahangiri and C. Sun, "Three-dimensional vibration control of offshore floating wind turbines using multiple tuned mass dampers," *Ocean Engineering*, vol. 206, Article ID 107196, 2020.

[30] Z. Lei, G. Liu, and M. Wen, "Vibration attenuation for offshore wind turbine by a 3D prestressed tuned mass damper considering the variable pitch and yaw behaviors," *Ocean Engineering*, vol. 281, Article ID 114741, 2023.

[31] W. Wang, X. Li, H. Zhao, B. Wang, and Y. Li, "Vibration control of a pentapod offshore wind turbine under combined seismic wind and wave loads using multiple tuned mass damper," *Applied Ocean Research*, vol. 103, Article ID 102254, 2020.

[32] D. Leng, Y. Yang, K. Xu et al., "Vibration control of offshore wind turbine under multiple hazards using single variable-stiffness tuned mass damper," *Ocean Engineering*, vol. 236, Article ID 109473, 2021.

[33] Z. Zhang, "Vibration suppression of floating offshore wind turbines using electromagnetic shunt tuned mass damper," *Renewable Energy*, vol. 198, pp. 1279–1295, 2022.

[34] A. Hemmati, E. Oterkus, and M. Khorasanchi, "Vibration suppression of offshore wind turbine foundations using tuned liquid column dampers and tuned mass dampers," *Ocean Engineering*, vol. 172, pp. 286–295, 2019.

[35] H. Zuo, K. Bi, and H. Hao, "Using multiple tuned mass dampers to control offshore wind turbine vibrations under multiple hazards," *Engineering Structures*, vol. 141, pp. 303–315, 2017.

[36] S. Adhikari and S. Bhattacharya, "Dynamic analysis of wind turbine towers on flexible foundations," *Shock and Vibration*, vol. 19, p. 20, Article ID 408493, 2012.

[37] L. Arany, S. Bhattacharya, S. J. Hogan, and J. Macdonald, "Dynamic soil-structure interaction issues of offshore wind turbines," in *Proceedings of the 9th International Conference on Structural Dynamics, EURODYN 2014*, A. Cunha, E. Caetano, P. Ribeiro, and G. Müller, Eds., pp. 3611–3617, Porto, Portugal, 2014.

[38] Y.-Y. Ko, "A simplified structural model for monopile-supported offshore wind turbines with tapered towers," *Renewable Energy*, vol. 156, pp. 777–790, 2020.

[39] R. W. Clough and J. Penzien, *Dynamics of Structures*, Higher Education Press, Beijing, 2006.

[40] C. B. Yang, "*The Regulation, control and evaluation of dynamic response for offshore wind turbine foundations*," Ph.D. Thesis, Tsinghua University, Beijing, China, 2017.

[41] J. Jonkman, S. Butterfield, W. Musial, and G. Scott, "Definition of a 5-MW reference wind turbine for offshore system development," *Technical Report*. NREL/TP-500-38060, National Renewable Energy Laboratory, USA, 2009.

[42] P. Alkhoury, A.-H. Soubra, V. Rey, and M. Aït-Ahmed, "A full three-dimensional model for the estimation of the natural frequencies of an offshore wind turbine in sand," *Wind Energy*, vol. 24, no. 7, pp. 699–719, 2021.

[43] C. Bak, F. Zahle, R. Bitsche et al., "Description of the DTU 10 MW reference wind turbine," pp. 1–138, 2013, DTU Wind energy report-I-0092, https://dtu-10mw-rwt.vindenergi.dtu.dk.

[44] H. G. Poulos and E. H. Davis, *Pile Foundation Analysis and Design*, Hongqiao Bookstore Co. Ltd, Taipei, 1981.

[45] A. B. Vesić, "Bending of beams resting on isotropic elastic solid," *Journal of the Engineering Mechanics Division*, vol. 87, no. 2, pp. 35–53, 1961.